TUTORIALS

A REVIEW OF DIGITAL BREAST TOMOSYNTHESIS

I. Reiser[1] and I. Sechopoulos[2]

[1] Department of Radiology, The University of Chicago, Chicago, IL, US
[2] Departments of Radiology and Imaging Sciences, Hematology and Medical Oncology and Winship Cancer Institute, Emory University, Atlanta, GA, US

Abstract— **While the principle of tomosynthesis has been known for almost a century, digital breast tomosynthesis (DBT) is a novel technology that owes its rapid development to the introduction of full-field digital mammography (FFDM). This review article covers the principles and design considerations of DBT, including system geometry. Further, the article provides an in-depth introduction to DBT dosimetry, and discusses recent studies on several breast imaging applications, which highlight the potential for clinical performance improvements due to DBT.**

Keywords— **Tomosynthesis, breast imaging, mammography, breast cancer**

I. Introduction

For the past decades, x-ray projection imaging of the breast, also known as mammography, has been the workhorse of the breast-imaging suite. Mammography is the recommended breast-cancer screening tool for most women. Breast cancer screening with mammography is estimated to account for about half of the 24% reduction in breast cancer mortality achieved between 1975 and 2000 [1]. A screening mammography exam consists of two anatomic projections along the cranio-caudal (CC) and mediolateral-oblique (MLO) directions for each breast.

Diagnostic mammography is the primary problem-solving tool for breast abnormalities. Its uses include the work-up of screen-detected findings, or the short-term follow-up of probably benign lesions, with a 31.4% positive predictive value for biopsy recommendations [2].

Despite these successes, mammography is limited by tissue superimposition. Overlaying dense tissues can mask tumors, potentially leading to a missed cancer. Furthermore, overlapping structures can mimic the appearance of a tumor and thereby cause a false-positive recall or biopsy. Tomosynthesis imaging has the potential to overcome these limitations by adding depth resolution to a mammogram [3–6]. In tomosynthesis, a sequence of projection views is acquired while the x-ray source travels along an arc. The projections are then reconstructed into a quasi-three-dimensional image volume. Conceptually, tomosynthesis could be considered a limited-angle CT scan.

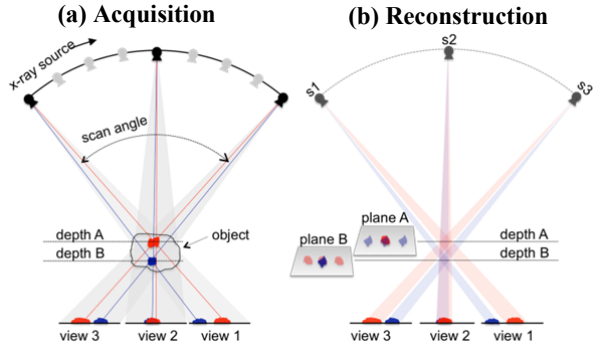

Fig. 1 (a) Tomosynthesis data acquisition and (b) shift-and-add image reconstruction. In this schematic, three source positions (s1-s3) are shown, while in an actual DBT unit, the number of projection views ranges between ~10 and 30 (see Table 1).

Tomosynthesis data acquisition and image reconstruction are shown schematically in Fig. 1. Within the object to be imaged, two structures are located at different depths, indicated by depth A and depth B (Fig. 1a). In each projection view, the x-ray source angle is different and therefore structures at different depths are projected onto different locations. Figure 1b shows an example of shift-and-add reconstruction: A reconstructed plane at a given depth in the object is obtained by adding all projection views. Depending on the imaging geometry, the projections are shifted and minified prior to summation. As seen in the reconstructed (i.e., tomosynthesis) planes A and B, the structure that is actually located at the corresponding depth is in-focus,

whereas the structure above or below is blurred. Thus, each reconstructed tomosynthesis plane contains image information from the entire object. This is different from a CT image, where structures outside the reconstructed image plane are removed entirely.

The principle of tomosynthesis was demonstrated as early as 1932 by Ziedses des Plantes [7]. Film-based clinical prototypes were built in the 1970s-1980s [8,9]. Digital breast tomosynthesis (DBT) was pioneered in the 1990s by Niklason, Kopans and colleagues [10,11], owing to advances in large-area flat-panel detector technologies [12]. Originally, these detectors were developed for use in full-field digital mammography (FFDM), which received approval by the Food and Drug Administration of the United States (FDA) in 2000. Piggybacking on these technological advances, digital breast tomosynthesis received FDA approval for use in breast cancer screening and diagnosis merely a decade later.

II. Image characteristics

The overall image appearance of a DBT image is similar to that of a conventional mammogram. Figures 2 and 3 show examples of benign and malignant breast masses imaged with mammography and tomosynthesis.

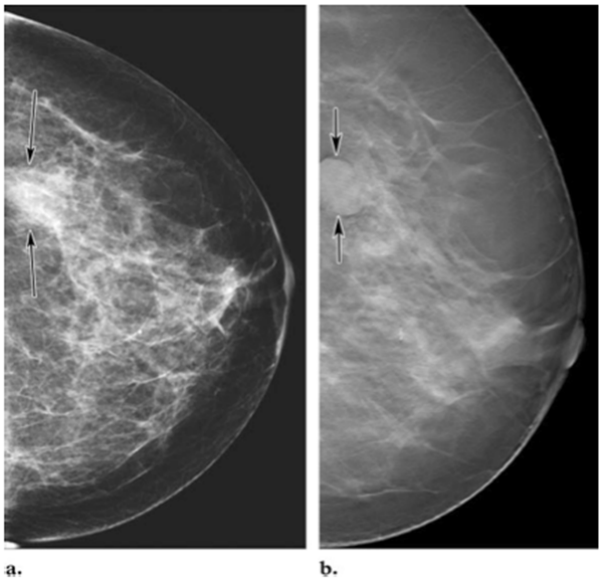

Fig. 2 (a) Mammogram and (b) tomosynthesis image of a benign breast mass (arrows) demonstrating enhanced visibility in the latter. Reproduced, with permission, from Park JM, Franken EA, Garg M, Fajardo, LL, Niklason, LT. Breast tomosynthesis: Present considerations and future applications. Radiographics, 2007, vol 27 Suppl. 1, pages S231–40.

The smooth margin of the benign mass in Fig. 2 is difficult to perceive in the mammogram because of overlaying densities that are projected onto the same location in the image. In the tomosynthesis image, the sharp lesion margin is clearly visualized, as confounding out-of-plane structures are removed (i.e., blurred).

In Figure 3, the tomosynthesis image reveals ductal infiltration by the cancer, which is not seen in the mammogram due to masking by overlapping fibroglandular tissue.

Thus, tomosynthesis potentially depicts benign lesions more clearly, decreasing recall rates, and reveals breast lesions that are not seen in a mammogram, thereby increasing breast cancer detection rates.

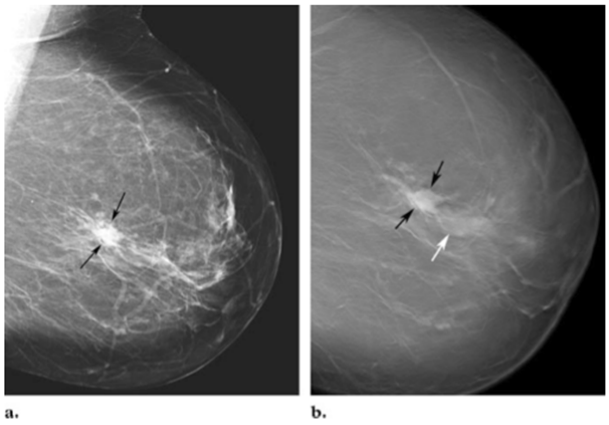

Fig. 3 (a) Mammogram and (b) tomosynthesis image of a malignant breast tumor (DCIS). Note the ductal extension of the cancer, seen only on tomosynthesis (white arrow). Reproduced, with permission, from Park JM, Franken EA, Garg M, Fajardo, LL, Niklason, LT. Breast tomosynthesis: Present considerations and future applications. Radiographics, 2007, vol 27 Suppl. 1, pages S231–40.

The spatial resolution of a tomosynthesis image volume is highly anisotropic. In planes parallel to the detector surface, resolution approximates that obtained by mammography, while depth resolution is poor. Due to the limited angle scan, depth resolution depends both on the scan angle (α) and the extent of an object along the scan direction. As a rule of thumb, an object of extent (x) persist across a depth (d) of about

$$d = x/\tan(\alpha/2) \quad (1)$$

Thus, depth resolution is better for small structures, i.e., microcalcifications typically only persist across a few tomosynthesis planes. Due to the highly anisotropic image volume, typical voxel dimensions in tomosynthesis are 100 μm x100 μm in-plane, and 1mm in-depth.

III. System design considerations

A large number of factors need to be considered when designing a DBT system. The basic components are

similar to those of a mammography system, such as the x-ray source and, for most systems, the flat-panel digital detector. Therefore, a DBT system can typically also be used for the acquisition of a conventional projection mammogram. In fact, the standard imaging protocol of the Hologic Selenia Dimensions system is to first acquire a FFDM, and then to retract the anti-scatter grid to perform a tomosynthesis scan, all while the breast is under compression. The total dose of this combined 2D + 3D imaging protocol is below the MQSA limit of 3 mGy per view when imaging the mammographic accreditation phantom.

However, actual requirements for tomosynthesis differ from those of a mammography system, and many represent trade-offs:

X-ray beam quality and gantry motion DBT systems tend to use higher x-ray tube potentials than what is used in FFDM, but with a relatively low-Z filter. Overall this produces x-ray beams with a lower effective energy, but allows for more efficient x-ray tube operation. [13]. The x-ray gantry for most tomosynthesis systems travels along an arc (for an in-depth discussion, see [3,14]). While the gantry moves, the x-ray beam can be continuously "on", or pulsed. Other systems employ a step-and-shoot operation (Table 1). The advantage of step-and-shoot over a continuous beam is the elimination of focal spot motion blur in the projection image. On the other hand, the overall acquisition time in a step-and-shoot system tends to be longer, making the system more susceptible to patient motion.

In most DBT systems, no anti-scatter grid is used because the source-detector geometry is different in each projection view. In some systems, the source-detector configuration remains constant during the scan [15]. This particular system has minimal scatter because it employs a slit-scanning photon counting detector. The GE SenoClaire is advertised to use an anti-scatter grid, but the actual implementation is proprietary.

X-ray detector The dose-dependence of the detector DQE is important in tomosynthesis systems, as the exposure to the detector per projection is at least an order of magnitude lower than that in FFDM [16]. Since electronic noise is independent of the detector entrance exposure, it can exceed quantum noise levels and reduce detection efficiency. In addition, temporal detector performance, such as lag and ghosting, needs to be considered. Electronic readout time should be below that of the overall scan time, and is sometimes reduced by pixel binning. In principle, photon-counting detectors are well suited for tomosynthesis because they do not exhibit electronic noise and have excellent temporal performance. Additionally, photon-counting detectors perform well in low count-rate applications, such as tomosynthesis [17,18]. Therefore, the Philips (Sectra) prototype DBT system uses a photon counting detector. Detectors for tomosynthesis are discussed in detail in [19].

Scan parameters The choice of the scan angle, and to a lesser amount the choice of number of views, greatly affect image quality of the tomosynthesis image. A number of investigators have studied the impact of these parameters on the detection performance over a range of signal sizes [20–24]. Consensus was found that increasing the scan angle increases the detectability of tumor-sized objects (~1cm diameter), while small scan angles improve detection of small-scale signals, such as microcalcifications and spiculations (Fig. 4). Current commercial DBT systems and prototypes utilize a wide variety of scan parameters (Table 1). The optimal parameter choice for DBT will likely depend on the physical factors of the system components, as well as the image reconstruction algorithm used. The clinical application may play a role as well.

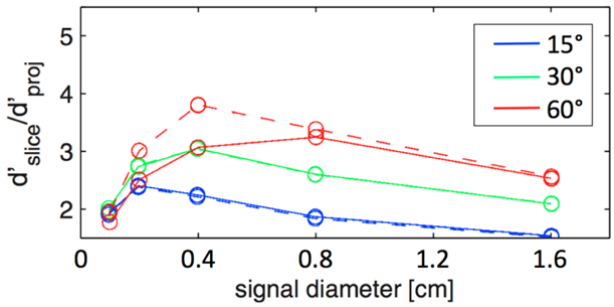

Fig. 4 Ratio of detectability index for a spherical signal in a DBT slice to that in a single projection, when an equal number of photons is used to acquire the tomosynthesis scan or the single projection, for scan angles of 15, 30 and 60, and 11 views (solid line) and 21 views (dashed line). These data are the result of a tomosynthesis simulation that assumed an ideal system, without degradation due to physical factors such as limited x-ray detection efficiency or detector blur. Details of the simulation can be found in [25] .

Image reconstruction The image reconstruction algorithm strongly affects the image quality in tomosynthesis imaging [26–28]. Early systems made use of modified filtered-back projection algorithms.

Table 1 Design parameters of commercial tomosynthesis units.

Model	scan angle (deg)	# of views	x-ray operation	scan time (sec)	Reconstruction algorithm
Hologic Selenia Dimensions*	15	15	continuous (pulsed)	4.5	FBP-based
Siemens MAMMOMAT Inspiration**	50	25	continuous (pulsed)	20	FBP-based
Giotto**	40	13	step-and-shoot with variable dose/view		iterative
GE SenoClaire**	24	9	step-and-shoot	7-10	iterative (ASIR)

* Approved for breast cancer screening and diagnosis by the Food and Drug Administration of the United States (US)

** CE mark

The appeal of this algorithm lies in its simplicity and short reconstruction time, but it can produce artifacts when the view sampling is sparse. Additional filtering is typically used to improve its performance in tomosynthesis [29,30]. Some DBT systems employ iterative reconstruction algorithms, which are better suited to reconstructions from limited angle, few-view projections (see Table 1) [28,31–33].

IV. Radiation dosimetry

In gross terms, the breast is composed of three types of tissue: glandular, adipose and skin. Since the risk of development of breast cancer in adipose tissue is minimal, breast radiation dosimetry is concerned only with the dose deposited in the glandular tissue of the breast. Therefore, since it was proposed by Hammerstein et al in 1979 [34], the metric of choice to estimate dose in x-ray breast imaging is the *mean glandular dose* (MGD, sometimes also referred to as the *average glandular dose* [AGD]), which means the absorbed dose to all the glandular tissue of the breast in the field of view. It is important to note that in breast imaging, due to the use of x rays of relatively low energy, the variation in the glandular dose deposited in different regions of the same breast during one acquisition can vary considerably with tissue depth [34–36].

One complicating factor for estimating the MGD is that although glandular tissue tends to be concentrated towards the center of the breast, the amount and spatial distribution of glandular and adipose tissue in a breast is random, and can vary widely among women. To avoid this complication, Hammerstein et al proposed that, for comparison purposes among techniques, the MGD be estimated assuming that the breast is composed of a homogeneous mixture of adipose and glandular tissue surrounded by a layer of skin [34]. Of course, since this definition of the breast tissue is not representative of any patient breast, Hammerstein et al stated that risk estimates should not be made from MGD. Recent studies have shown that using MGD to a homogeneous breast as an estimate of absorbed dose to the glandular tissue portion of an actual patient's breast can result in large errors [37,38]. For two reasons, however, the use of the MGD with the homogeneous breast assumption has become the *de facto* standard in breast dosimetry. In the first place, it is very challenging to estimate the actual MGD to an actual patient breast considering its real tissue distribution. In addition, for most applications having a relative, rather than an absolute, dose estimate is sufficient. Specifically, for quality control and assurance, technique optimization and comparison of imaging technologies, having a metric that correlates with risk and is relatively easy to estimate is not only sufficient, but desirable. Therefore, the MGD and how it varies with patient and imaging system characteristics has been studied extensively in mammography [39–44].

Of course, these studies do not actually provide and analyze values for MGD, but rather for its normalized version, the *normalized glandular dose* (D_gN). This metric is simply the MGD normalized by the air kerma (or exposure) at the top surface of the breast (on the side where the x rays are incident). The D_gN can be thought of as the conversion factor from entrance air kerma to MGD. From the studies of D_gN in mammography it is known that this conversion factor is a function of breast thickness, glandular density and x-ray spectrum [39–44]. In DBT, the impact on D_gN of a new acquisition parameter, the projection angle, was studied by Sechopoulos et al [45,46]. In those studies, the authors found that the impact of the projection angle on D_gN varies only with breast thickness and size, and is mostly independent of glandular density and x-ray spectrum. Therefore, Sechopoulos et al proposed that for calculation of MGD in DBT imaging, the D_gN data for mammography could be used with the addition of a new factor, the *relative glandular dose* (RGD), which introduces the variation in D_gN due to the variation in position of the x-ray tube during tomosynthesis acquisition. Therefore, the RGD was defined as:

$$RGD(\alpha) = \frac{\mathrm{D}_g\mathrm{N}(\alpha)}{\mathrm{D}_g\mathrm{N}(0°)} \quad (2)$$

where α is the tomosynthesis projection angle. As is apparent, $D_gN(0°)$ is equivalent to the mammographic D_gN for the equivalent acquisition parameters (breast characteristics and x-ray spectrum). With this definition of RGD, the MGD for a complete tomosynthesis acquisition can be estimated using:

$$MGD = ESAK_0 \cdot DgN_0 \cdot \sum_N RGD(\alpha) \quad (3)$$

where $ESAK_0$ is the entrance surface air kerma for the zero-degree projection (equivalent to the mammography acquisition geometry), D_gN_0 is the mammographic D_gN conversion factor, and the sum of RGD is over all N projection angles included in the tomosynthesis acquisition. This equation can be re-written as:

$$MGD = ESAK_0 \cdot DgN_0 \cdot N \cdot \overline{RGD} \quad (4)$$

where, as before, N is the number of projections included in the tomosynthesis acquisition and $\overline{\mathrm{RGD}}$ is the mean of all N RGDs for the projection angles involved in the tomosynthesis acquisition. Since, as mentioned, RGD is independent of breast density and x-ray spectrum, for a specific tomosynthesis system, and therefore for a known distribution of projection angles, $\overline{\mathrm{RGD}}$ for each specific breast thickness can be

calculated beforehand and provided in a table. Sechopoulos et al [45,46] provided tables for D_gN_0 and fit equations for RGD for breast tomosynthesis imaging in the CC and MLO views. The upcoming Report of Task Group 223 of the American Association of Physicists in Medicine (in print) will provide RGD values for a generic tomosynthesis system and the $\overline{RGD}$ values for a number of commercial and advanced prototype tomosynthesis systems using as a basis the Wu et al model for mammography breast dosimetry commonly used in the US [40,41].

Similar modifications to the mammography breast dosimetry model developed by Dance et al and used in the United Kingdom, Europe and by the International Atomic Energy Agency [39,43,47] were made for DBT, as described by Dance et al [48]. In that nomenclature, RGD is replaced by t, while $\overline{RGD}$ is replaced by T, but their definition is equivalent. In this work, Dance et al provide values for t and T for generic systems and values for T for three currently commercial and advanced prototype DBT systems [48]. Additional tabular values for normalized glandular dose for x-ray tubes with tungsten targets were provided by Ma et al [49]. Ma et al also studied how these values vary with varying positioning of the breast on the detector, finding that this can cause a variation in dose of up to 13%.

All the above publications that studied and provided values for D_gN and RGD (or t and T) allow for the calculation of MGD for breast tomosynthesis for a given acquisition condition. They do not, however, provide information on the radiation dose involved in tomosynthesis acquisition in absolute terms, and therefore do not provide the information necessary to compare the actual glandular dose used in DBT to that used in other modalities, such as conventional mammography. To obtain dose values in absolute terms and be able to compare the dose involved in DBT with other breast imaging modalities, it is necessary to characterize the ESAK used by the imaging system to acquire an image. Of course, in a clinical system this value will depend on the settings of the automatic exposure control (AEC), which will vary the tube voltage and the tube current-exposure time product (and in some systems the additional filter) depending on the imaged breast characteristics. Typically, the compressed breast thickness is used to set the tube voltage, while the breast glandular density is probed with a low-dose scout image to set the tube current-exposure time product. Depending on the AEC system, it may also vary the tube voltage based on the results of the scout image. Given this variation in acquisition parameters with breast characteristics, to be able to study the MGD in tomosynthesis it is necessary to characterize the AEC system behavior. For this, Feng and Sechopoulos used custom-made homogeneous breast phantoms of varying thickness and equivalent breast density to probe the acquisition settings used by a commercial DBT system to acquire both tomosynthesis and mammography images [50]. Using an ion chamber and a dosimeter they were able to obtain ESAK values for the range of equivalent breasts investigated, and, in combination with these values, Monte Carlo-based D_gN_0 and RGD values were used to estimate MGD for these breasts. The authors found that in the majority of cases the MGD from tomosynthesis was higher than that for mammographic acquisition, and that for an average breast defined as 5 cm thick with 50% glandular density the increase was minimal (8%). However, for a newer definition of an average breast (6 cm thick and ~15% glandular density), the difference was larger (83%). It was also found that given the advances in system technology, the overall MGD for a combined mammography/tomosynthesis study is similar to that used for digital mammography alone just a few years earlier on previous generation systems [51]. The Feng and Sechopoulos study was exclusively breast phantom-based, and, as the authors suggested, it is of interest to compare MGD estimates for mammography and DBT based on acquisition parameters used for a large number of actual patients, data that was not available at the time. In the same year, Strudley et al reported on quality control procedures used during the TOMMY trial, a multi-site patient trial performed in the United Kingdom [52]. These tests included estimation of the MGD used by the Hologic Selenia Dimensions systems used in this trial for different breast equivalent phantoms, and they found similar relationships between mammography and tomosynthesis MGD as those reported by Feng and Sechopoulos [50].

In the first study using patient data to characterize MGD in tomosynthesis, Dance et al tested the appropriateness of the tomosynthesis dosimetry model proposed for the European guidelines discussed above by comparing the MGD estimates following the proposed protocol with polymethyl methacrylate (PMMA) phantoms to those obtained when imaging a total of 541 patients with two different commercial DBT systems [53]. The authors found that the use of the phantoms resulted in a reasonable estimate of MGD for patients (of course, still assuming the homogeneous tissue mixture approximation). In addition, they found a relationship between mammography and tomosynthesis MGD similar to that previously reported by Feng and Sechopoulos and Strudley et al.

Cavagnetto et al also studied the entrance surface air kerma and MGD from mammography and tomosynthesis, using the UK/IAEA breast dosimetry model and data on the image acquisition parameters selected by the AEC system during acquisition of 300 patient mammography and tomosynthesis combined exams with a commercial system [54]. The authors found similar increases in MGD when comparing the tomosynthesis to the mammography acquisitions as those reported by Feng and Sechopoulos

and Strudley et al using phantoms and Dance et al using patient data. In addition to this comparison, in the same study, Cavagnetto et al investigated the feasibility of using metal oxide semiconductor field effect transistor (MOSFET) dosimeters to measure ESAK in real time during combined acquisition of a mammography and tomosynthesis exam for each patient. The authors found that the use of such detectors is feasible, but that for low tube current-exposure time products, such as those used for compressed breast thicknesses below 30 mm, the measurement noise results in higher-than-desirable uncertainties in the measurement. However, the authors point out that this would typically affect only about 2% of the population of compressed breasts.

In the initial commercial implementation of DBT in the United States, the acquisition of a complete breast screening exam included the acquisition of both a standard 2D mammogram and the tomosynthesis projections. This resulted in an increase in the glandular dose from screening as reflected in the works discussed above. More recently, the introduction of a "synthetic" mammogram, as discussed below [55], eliminates the need to acquire the mammogram in addition to the tomosynthesis projections, substantially reducing the dose involved in screening with DBT.

To aid in the estimation of MGD for DBT acquisitions, especially during testing for quality assurance and/or control in the clinical realm, Li et al compiled the data presented in tabular form from the various studies discussed above [37,39,43,45–47,50] and from the quality control manual of a commercial DBT system [56] and performed various parameterizations of the different models [57]. This allowed the authors to provide easy-to-use electronic spreadsheets that permit the user to enter the appropriate inputs (e.g. breast thickness, tube voltage), with the spreadsheet providing the value of the corresponding factor (e.g. D_gN in the case of the US-based data or g, c, s, and t factors for the UK/IAEA data). This avoids the need for the user to perform any interpolation of results from tabular data.

Finally, the introduction of non-normal incidence of x-rays during tomosynthesis acquisition can necessitate modifications to the AEC behavior testing during dosimetry quality assurance and control procedures. To address this, Bouwman et al [58,59] have introduced a new set of phantoms, based on PMMA and polyethylene (PE) slabs of varying thicknesses. These are equivalent to the set of "standard breasts" [43] used in the European Guidelines for quality assurance in breast cancer screening and diagnosis [60] but resolve the possible issues encountered in tomosynthesis with the previous methodology.

V. Clinical studies

In 2007, initial studies by Poplack et al. and Rafferty et al. found breast lesions to be more conspicuous on DBT than on conventional mammograms [61,62]. Subsequently, several reader studies used enriched datasets (i.e., a mix of patient cases in which the cancer prevalence is higher than in a screening population) to investigate the diagnostic performance of DBT. Based on 125 patient cases, 35 of which had verified breast cancer, Gur et al. found a 30% reduction in recall rate when combining mammography with DBT, compared to mammography alone [63]. In this early study, no benefit in sensitivity was found. Gennaro et al compared single-view DBT (MLO) to two-view mammography. Based on images from 200 patients with at least one breast lesion, she concluded that DBT performance was not inferior to mammography [64]. Svahn et al. found higher sensitivity for single-view DBT, compared to two-view FFDM, without significant changes in specificity [65].

Breast cancer screening with DBT Subsequent larger studies on screening populations corroborated the findings of increased sensitivity and reduced recall rate. After introducing routine screening with DBT to their practice, Rose et al report a reduction of recall rate from 8.7% to 5.5%, based on 13856 women screened with mammography and 9499 women screened with mammography plus tomosynthesis [66]. In a retrospective study that reviewed screening mammograms from 13158 women and screening mammography plus tomosynthesis from 6100 women, Haas and colleagues found a 30% decrease in recall rate in women screened with mammography alone (12.0%), compared to women screened with mammography plus tomosynthesis (8.4%) [67]. The cancer detection rate was greater for mammography plus tomosynthesis than for mammography alone, but the difference was not statistically significant. A decrease in recall rate was observed for all breast densities, with statistical significance for all densities except for predominantly fatty, which is the breast density for which mammography sensitivity is highest [68]. Likely, the difference in cancer detection rate failed to reach significance because of the relatively smaller number of cancers compared to the number of recalls, which requires a larger number of women participating in a study.

Skaane et al. reported interim results of a prospective screening study (i.e., the Oslo tomosynthesis screening trial), which included 12631 women that were screened within a timeframe of roughly one year. A 31% increase in cancer detection rate for mammography plus tomosynthesis (8.0/1000) was found, compared to mammography alone (6.1/1000) [69]. The false positive rate for mammography plus tomosynthesis was 5.31%, a 13% reduction compared to that for mammography alone (6.11%). This more modest reduction in recall rate in

comparison to the study by Rose et al and Haas et al may be due to differences in cancer screening strategies in Europe and the United States [70]. However, this interim analysis also found that the mean interpretation time doubled, from an average of 45 sec for mammography alone to about 90 sec for mammography plus DBT.

Diagnostic imaging with DBT Hakim et al. performed a preference study comparing DBT with additional mammographic views [71]. In 81% of the cases, combined FFDM and DBT was perceived to be equal or better for diagnosis. This study did not include cases with microcalcifications alone. The workup of screening recalls with DBT was investigated by Brandt et al., who found that assessment with DBT was highly correlated with that of clinical work-up with additional mammographic views, in a cohort of 146 women with abnormalities (excluding calcifications) [72]. Zuley et al. found that diagnostic performance in terms of area under the ROC curve (AUC) improved significantly when DBT was used instead of additional mammographic views, based on 182 cases that included 217 noncalcified lesions [73].

Comparing DBT alone with FFDM and FFDM plus DBT, Thibault et al. and Gennaro et al. were able to show non-inferiority of DBT alone, using patient data from a GE prototype [64,74]. Foernvik and colleagues found DBT alone to be more accurate for the assessment of lesion size than FFDM, significantly improving the accuracy of tumor staging [75]. Actual lesion sizes were verified by ultrasound imaging, and DBT imaging was performed with a Siemens system. Mun et al. found similar improvements with a GE DBT prototype [76].

Visualization of microcalcifications with DBT Spangler and colleagues performed an investigation of microcalcification imaging with DBT [77]. Their study included 100 cases with 60 microcalcification clusters (40 benign, 20 malignant). The remaining 40 cases were normal. The four standard mammographic views, i.e., CC and MLO images of both breasts, were available for both FFDM and DBT. Patient cases were acquired using the Hologic Selenia Dimensions DBT system. Microcalcification detection sensitivity was higher with FFDM. This finding held for all microcalcifications, as well as for both benign and malignant clusters individually. For calcification clusters that were detected on both modalities, the difference in AUC in the task of distinguishing benign from malignant clusters was not statistically significant. Note that the tomosynthesis display did allow for "slab-viewing".

On the other hand, Kopans et al report that conspicuity of microcalcifications was equal to or better than FFDM in 92% of 119 sequential cases with calcifications [78]. The patient images used in this study were acquired on a GE prototype unit, at a dose equivalent to that of two screen-film mammograms.

These apparently inconsistent findings could be due to differences in study design – the first study being an ROC study, whereas the latter study was a subjective preference study. Furthermore, patient data for the studies was collected on different DBT units, operated at different dose levels, and, perhaps importantly, with different scanning modes (i.e. continuous pulsed vs. step-and-shoot). Further research is needed to clarify whether DBT image quality is sufficient for microcalcification imaging.

VI. Practical considerations

One view or two view DBT? Since DBT is a tomographic modality, presumably a single DBT view might provide sufficient depth information, so that a second DBT view might not be needed.

Anderson et al. investigated the detection of subtle breast masses with DBT in a small study that included 44 cancers in 37 breasts, using a Siemens prototype DBT system [79]. For each breast, a single-view DBT scan as well as two-view mammograms were available. 22 masses were more visible on DBT than single-view mammography, and the BIRADS score of 21 masses was upgraded. In comparison with two-view mammography, 11 masses were more visible on DBT, and BIRADS scores of 12 masses were upgraded. Wallis et al. compared two-view mammography with one or two-view DBT, using the SECTRA microdose DBT system [80]. Improvement was found for two-view DBT, but not for single-view DBT. In two studies using patient data acquired on a GE prototype, both Gennaro et al. and Thibault et al. found that single-view DBT was not inferior to two-view FFDM [74,81].

Synthetic 2D The original FDA-approved imaging sequence of the Hologic Selenia Dimensions unit consisted of the acquisition of a conventional FFDM image, followed by the DBT scan. In order to reduce patient dose, Hologic introduced the use of a *synthetic 2D* image to replace the FFDM acquisition. This synthetic *2D* image is generated from the tomosynthesis dataset, making the acquisition of the conventional mammogram obsolete, and thereby reducing radiation dose substantially. The "synthetic 2D" image is processed to emphasize suspicious structures in individual DBT slices, rather than to approximate a mammographic projection. In 2013, the FDA approved the replacement of the FFDM image from the combined FFDM-tomosynthesis exam with a synthetic 2D.

Two recent studies by Skaane et al. and Zuley et al. report similar performance when readers used FFDM or synthetic 2D [82,83]. With an earlier version of the synthetic 2D, Gur et al. found a slight decrease in cancer detection sensitivity, but no change in recall rate [55].

A method to generate synthetic 2D images that enhance lesion characteristics is described by Schie et al [84]. Note that this is not the algorithm used by Hologic. The use of synthetic 2D may also prove useful for comparison with prior mammograms or DBT images.

Reading time Several studies report significant increases in reading time with DBT [63,85,86]. Given the low prevalence of breast cancer in screening populations with about 5 cancers per 1000 screening exams, longer reading times will reduce the cost-effectiveness of breast cancer screening. Computer-aided detection schemes may potentially help offset the reduction in productivity [87–90].

VII. CONCLUSIONS

DBT is an emerging tomographic modality for breast imaging that may potentially replace conventional projection mammography both for breast cancer screening and diagnosis. Current clinical studies are promising and indicate the potential for increased cancer detection sensitivity and reduced recall rates. However, several issues need to be addressed to better integrate DBT into the clinical environment, such as the development of efficient viewing strategies. Further, if DBT is to replace FFDM, its clinical performance in lesions with microcalcifications needs to be ascertained and possibly improved.

ACKNOWLEDGMENT

The authors would like to acknowledge assistance with editing by Jessica Paulishen.

REFERENCES

1. Berry DA, Cronin KA, Plevritis SK, et al. (2005) Effect of screening and adjuvant therapy on mortality from breast cancer. NEJM 353: 1784–1792. doi:10.1056/NEJMoa050518.
2. Sickles EA, Miglioretti DL, Ballard-Barbash R, et al. (2005) Performance benchmarks for diagnostic mammography. Radiology 235: 775–790. doi:10.1148/radiol.2353040738.
3. Dobbins, III JT, Godfrey DJ (2003) Digital x-ray tomosynthesis: current state of the art and clinical potential. Phys Med Biol 48: R65–106.
4. Baker JA, Lo JY (2011) Breast tomosynthesis: state-of-the-art and review of the literature. Acad Radiol 18: 1298–1310. doi:10.1016/j.acra.2011.06.011.
5. Sechopoulos I (2013) A review of breast tomosynthesis. Part I. The image acquisition process. Med Phys 40: 014301–014301–12. doi:10.1118/1.4770279.
6. Sechopoulos I (2013) A review of breast tomosynthesis. Part II. Image reconstruction, processing and analysis, and advanced applications. Med Phys 40: 014302–014302–17. doi:10.1118/1.4770281.
7. Des Plantes Z (1932) Eine neue Methode zur Differenzierung in der Roentgenographie (Planigraphie). Acta Radiol 13: 182–192.
8. Grant D (1972) Tomosynthesis: A three-dimensional radiographic imaging technique. IEEE Trans BME 19: 20–28.
9. Woelke H, Hanrath P, Schlueter M, et al. (1982) Work in progress. Flashing tomosynthesis: a tomographic technique for quantitative coronary angiography. Radiology 145: 357–360.
10. Niklason T, Christian BT, Niklason LE, et al. (1997) Digital Tomosynthesis in Breast Imaging. Radiology 205: 399–406.
11. Wu T, Stewart A, Stanton M, et al. (2003) Tomographic mammography using a limited number of low-dose cone-beam projection images. Med Phys 30: 365–380. doi:10.1118/1.1543934.
12. Suryanarayanan S, Karellas A, Vedantham S (2004) Physical characteristics of a full-field digital mammography system. NIM B 533: 560–570. doi:10.1016/j.nima.2004.05.128.
13. Feng SSJ, Sechopoulos I (2012) Clinical Digital Breast Tomosynthesis System: Dosimetric Characterization. Radiology 263: 35–42.
14. Glick SJ (2014) System design and acquisition parameters for tomosynthesis. In: Reiser IS, Glick SJ, editors. Tomosynthesis Imaging. Taylor & Francis.
15. Svane G, Azavedo E, Lindman K, et al. (2011) Clinical experience of photon counting breast tomosynthesis: comparison with traditional mammography. Acta Radiol 52: 134–142. doi:10.1258/ar.2010.100262.
16. Zhao B, Zhao W (2008) Imaging performance of an amorphous selenium digital mammography detector in a breast tomosynthesis system. Med Phys 35: 1978. doi:10.1118/1.2903425.
17. Aslund M, Cederstroom B, Lundqvist M, et al. (2007) Physical characterization of a scanning photon counting digital mammography system based on Si-strip detectors. Med Phys 34: 1918–1925. doi:10.1118/1.2731032.
18. Fredenberg E, Lundqvist M, Åslund M, et al. (2009) A photon-counting detector for dual-energy breast tomosynthesis. Proc SPIE 7258. p. 72581J–72581J–11. doi:10.1117/12.813037.
19. Zhao W (2014) Detectors for tomosynthesis. In: Reiser IS, Glick SJ, editors. Tomosynthesis Imaging. Taylor & Francis.
20. Sechopoulos I, Ghetti C (2009) Optimization of the acquisition geometry in digital tomosynthesis of the breast. Med Phys 36: 1199–1207. doi:10.1118/1.3090889.
21. Chawla AS, Lo JY, Baker J a., et al. (2009) Optimized image acquisition for breast tomosynthesis in projection and reconstruction space. Med Phys 36: 4859–4869. doi:10.1118/1.3231814.
22. Reiser I, Joseph SP, Nishikawa RM, et al. (2010) Evaluation of a 3D lesion segmentation algorithm on tomosynthesis and breast CT images. Proc. SPIE. Vol. 7624. pp. 7624–7695.
23. Gang GJ, Tward DJ, Lee J, et al. (2010) Anatomical background and generalized detectability in tomosynthesis and cone-beam CT. Med Phys 37: 1948–1965. doi:10.1118/1.3352586.
24. Young S, Bakic PR, Myers KJ, et al. (2013) A virtual trial framework for quantifying the detectability of masses in breast tomosynthesis projection data. Med Phys 40: 051914–1–15. doi:10.1118/1.4800501.
25. Reiser I, Nishikawa RM (2010) Task-based assessment of breast tomosynthesis: Effect of acquisition parameters and quantum noise. Med Phys 37: 1591–1600. doi:10.1118/1.3357288.
26. Wu T, Moore RH, Rafferty EA, et al. (2004) A comparison of reconstruction algorithms for breast tomosynthesis. Med Phys 31: 2636–2647. doi:10.1118/1.1786692.
27. Zhang Y, Chan H-P, Sahiner B, et al. (2006) A comparative study of limited-angle cone-beam reconstruction methods for breast tomosynthesis. Med Phys 33: 3781–3795. doi:10.1118/1.2237543.
28. Sidky EY, Pan X, Reiser IS, et al. (2009) Enhanced imaging of microcalcifications in digital breast tomosynthesis through

improved image-reconstruction algorithms. Med Phys 36: 4920–4932. doi:10.1118/1.3232211.
29. Mertelmeier T, Orman J, Haerer W, et al. (2006) Optimizing filtered backprojection reconstruction for a breast tomosynthesis prototype device. Proc. SPIE. Vol. 6142. p. 61420F. doi:10.1117/12.651380.
30. Mertelmeier T (2014) Filtered backprojection-based methods for tomosynthesis image reconstruction. In: Reiser IS, Glick SJ, editors. Tomosynthesis Imaging. Taylor & Francis.
31. Reiser I, Bian J, Nishikawa R, et al. (2007) Comparison of reconstruction algorithms for digital breast tomosynthesis. 9th International Meeting on Fully Three-Dimensional Image Reconstruction in Radiology and Nuclear Medicine July 9 - 13, 2007, Lindau, Germany.
32. Zhang Y, Chan HP, Sahiner B, et al. (2006) Tomosynthesis reconstruction using the simultaneous algebraic reconstruction technique (SART) on breast phantom data. Proc. SPIE. Spie, Vol. 6142. p. 614249. doi:10.1117/12.654891.
33. Sidky EY (2014) Iterative image reconstruction design for digital breast tomosynthesis. In: Reiser IS, Glick SJ, editors. Tomosynthesis Imaging. Taylor & Francis.
34. Hammerstein GR, Miller DW, White DR, et al. (1979) Absorbed radiation dose in mammography. Radiology 130: 485–491.
35. Sechopoulos I, Feng SSJ, D'Orsi CJ (2010) Dosimetric characterization of a dedicated breast computed tomography clinical prototype. Med Phys 37: 4110–4120. doi:10.1118/1.3457331.
36. Samei E, Li X, Chen B, et al. (2013) The effect of dose heterogeneity on radiation risk in medical imaging. Radiat Prot Dosimetry 155: 42–58. doi:10.1093/rpd/ncs275.
37. Dance DR, Hunt RA, Bakic PR, et al. (2005) Breast dosimetry using high-resolution voxel phantoms. Radiat Prot Dosimetry 114: 359–363. doi:10.1093/rpd/nch510.
38. Sechopoulos I, Bliznakova K, Qin X, et al. (2012) Characterization of the homogeneous tissue mixture approximation in breast imaging dosimetry. Med Phys 39: 5050–5059.
39. Dance DR (1990) Monte Carlo calculation of conversion factors for the estimation of mean glandular breast dose. Phys Med Biol 35: 1211–1219.
40. Wu X, Barnes GT, Tucker DM (1991) Spectral dependence of glandular tissue dose in screen-film mammography. Radiology 179: 143–148.
41. Wu X, Gingold EL, Barnes GT, et al. (1994) Normalized average glandular dose in molybdenum target-rhodium filter and rhodium target-rhodium filter mammography. Radiology 193: 83–89.
42. Boone JM (1999) Glandular breast dose for monoenergetic and high-energy X-ray beams: Monte Carlo assessment. Radiology 213: 23–37.
43. Dance DR, Skinner CL, Young KC, et al. (2000) Additional factors for the estimation of mean glandular breast dose using the UK mammography dosimetry protocol. Phys Med Biol 45: 3225–3240.
44. Boone JM (2002) Normalized glandular dose (DgN) coefficients for arbitrary X-ray spectra in mammography: Computer-fit values of Monte Carlo derived data. Med Phys 29: 869–875.
45. Sechopoulos I, Suryanarayanan S, Vedantham S, et al. (2007) Computation of the glandular radiation dose in digital tomosynthesis of the breast. Med Phys 34: 221–232.
46. Sechopoulos I, D'Orsi CJ (2008) Glandular radiation dose in tomosynthesis of the breast using tungsten targets. J Appl Clin Med Phys 9: 161–171.
47. Dance DR, Young KC, Engen RE van (2009) Further factors for the estimation of mean glandular dose using the United Kingdom, European and IAEA breast dosimetry protocols. Phys Med Biol 54: 4361–4372.
48. Dance DR, Young KC, van Engen RE (2011) Estimation of mean glandular dose for breast tomosynthesis: factors for use with the UK, European and IAEA breast dosimetry protocols. Phys Med Biol 56: 453–471.
49. Ma AKW, Darambara DG, Stewart A, et al. (2008) Mean glandular dose estimation using MCNPX for a digital breast tomosynthesis system with tungsten/aluminum and tungsten/aluminum + silver x-ray anode-filter combinations. Med Phys 35: 5278–5289.
50. Feng S, Sechopoulos I (2012) Clinical digital breast tomosynthesis system: dosimetric characterization. Radiology 263: 35–42.
51. Hendrick RE, Pisano ED, Averbukh A, et al. (2010) Comparison of Acquisition Parameters and Breast Dose in Digital Mammography and Screen-Film Mammography in the American College of Radiology Imaging Network Digital Mammographic Imaging Screening Trial. Am J Roentgenol 194: 362–369. doi:10.2214/ajr.08.2114.
52. Strudley CJ, Young KC, Oduko JM, et al. (2012) Development of a Quality Control Protocol for Digital Breast Tomosynthesis Systems in the TOMMY Trial. In: Maidment ADA, Bakic PR, Gavenonis S, editors. IWDM 2012. Philadelphia, PA: Springer Berlin Heidelberg, Vol. 7361. pp. 330–337. doi:10.1007/978-3-642-31271-7_43.
53. Dance DR, Strudley CJ, Young KC, et al. (2012) Comparison of Breast Doses for Digital Tomosynthesis Estimated from Patient Exposures and Using PMMA Breast Phantoms. In: Maidment ADA, Bakic PR, Gavenonis S, editors. IWDM 2012. Philadelphia, PA: Springer Berlin Heidelberg, Vol. 7361. pp. 316–321. doi:10.1007/978-3-642-31271-7_41.
54. Cavagnetto F, Taccini G, Rosasco R, et al. (2013) "In vivo" average glandular dose evaluation: one-to-one comparison between digital breast tomosynthesis and full-field digital mammography. Radiat Prot Dosimetry 157: 53–61. doi:10.1093/rpd/nct120.
55. Gur D, Zuley ML, Anello MI, et al. (2012) Dose reduction in digital breast tomosynthesis (DBT) screening using synthetically reconstructed projection images: an observer performance study. Acad Radiol 19: 166–171. doi:10.1016/j.acra.2011.10.003.
56. Hologic Inc. (2011) Appendix C. Selenia Dimensions Quality Control Manual, Revision 002. Bedford, MA: Hologic Inc.
57. Li X, Zhang D, Liu B (2013) A parameterization method and application in breast tomosynthesis dosimetry. Med Phys 40: 92105. doi:doi:http://dx.doi.org/10.1118/1.4818059.
58. Bouwman R, Diaz O, Young K, et al. (2012) Phantoms for Quality Control Procedures of Digital Breast Tomosynthesis. IWDM 2012 7361: 322–329. doi:10.1007/978-3-642-31271-7_42.
59. Bouwman RW, Diaz O, Engen RE van, et al. (2013) Phantoms for quality control procedures in digital breast tomosynthesis: dose assessment. Phys Med Biol 58: 4423–4438.
60. Van Engen RE, Bosmans H, Dance DR, et al. (2013) Digital mammography update. European protocol for the quality control of the physical and technical aspects of mammography screening S1: part 1. Acceptance and constancy testing. In: Perry N, Broeders M, Wolf C de, et al., editors. European Guidelines for Quality Assurance in Breast Cancer Screening and Diagnosis. Luxembourg: Office for Official Publications of the European Communities. pp. 105–165.
61. Poplack SP, Tosteson TD, Kogel CA, et al. (2007) Digital breast tomosynthesis: initial experience in 98 women with abnormal digital screening mammography. AJR 189: 616–623. doi:10.2214/AJR.07.2231.
62. Rafferty EA (2007) Digital mammography: novel applications. Radiol Clin North Am 45: 831–843. doi:10.1016/j.rcl.2007.06.005.
63. Gur D, Abrams GS, Chough DM, et al. (2009) Digital breast tomosynthesis: observer performance study. AJR 193: 586–591. doi:10.2214/AJR.08.2031.
64. Gennaro G, Toledano A, di Maggio C, et al. (2010) Digital breast tomosynthesis versus digital mammography: a clinical

performance study. Eur Radiol 20: 1545–1553. doi:10.1007/s00330-009-1699-5.
65. Svahn TM, Chakraborty DP, Ikeda D, et al. (2012) Breast tomosynthesis and digital mammography: a comparison of diagnostic accuracy. Br J Radiol: 1–9. doi:10.1259/bjr/53282892.
66. Rose SL, Tidwell AL, Bujnoch LJ, et al. (2013) Implementation of breast tomosynthesis in a routine screening practice: an observational study. AJR 200: 1401–1408. doi:10.2214/AJR.12.9672.
67. Haas BM, Kalra V, Geisel J, et al. (2013) Comparison of tomosynthesis plus digital mammography and digital mammography alone for breast cancer screening. Radiology 269: 694–700. doi:10.1148/radiol.13130307.
68. Mandelson M (2000) Breast density as a predictor of mammographic detection: comparison of interval-and screen-detected cancers. J Natl Cancer Inst 92: 1081–1087.
69. Skaane P, Bandos AI, Gullien R, et al. (2013) Comparison of Digital Mammography Alone and Digital Mammography Plus Tomosynthesis in a Population-based Screening Program. Radiology 267: 47–56.
70. Hofvind S, Vacek PM, Skelly J, et al. (2008) Comparing screening mammography for early breast cancer detection in Vermont and Norway. J Natl Cancer Inst 100: 1082–1091. doi:10.1093/jnci/djn224.
71. Hakim CM, Chough DM, Ganott MA, et al. (2010) Digital breast tomosynthesis in the diagnostic environment: A subjective side-by-side review. AJR 195: W172–6. doi:10.2214/AJR.09.3244.
72. Brandt KR, Craig DA, Hoskins TL, et al. (2013) Can Digital Breast Tomosynthesis Replace Conventional Diagnostic Mammography Views for Screening Recalls Without Calcifications? A Comparison Study in a Simulated Clinical Setting. AJR 200: 291–298. doi:10.2214/AJR.12.8881.
73. Zuley ML, Bandos AI, Ganott MA, et al. (2013) Digital breast tomosynthesis versus supplemental diagnostic mammographic views for evaluation of noncalcified breast lesions. Radiology 266: 89–95. doi:10.1148/radiol.12120552.
74. Thibault F, Dromain C, Breucq C, et al. (2013) Digital breast tomosynthesis versus mammography and breast ultrasound: a multireader performance study. Eur Radiol 23: 2441–2449. doi:10.1007/s00330-013-2863-5.
75. Förnvik D, Zackrisson S, Ljungberg O, et al. (2010) Breast tomosynthesis: Accuracy of tumor measurement compared with digital mammography and ultrasonography. Acta Radiol 51: 240–247. doi:10.3109/02841850903524447.
76. Mun HS, Kim HH, Shin HJ, et al. (2013) Assessment of extent of breast cancer: comparison between digital breast tomosynthesis and full-field digital mammography. Clin Radiol 68: 1254–1259. doi:10.1016/j.crad.2013.07.006.
77. Spangler ML, Zuley ML, Sumkin JH, et al. (2011) Detection and Classification of Calcifications on Digital Breast Tomosynthesis and 2D Digital Mammography: A Comparison. AJR 196: 320–324. doi:10.2214/AJR.10.4656.
78. Kopans D, Gaveonis S, Halpern E, et al. (2011) Calcifications in the Breast and Digital Breast Tomosynthesis. Breast J 17: 638–644. doi:10.1111/j.1524-4741.2011.01152.x.
79. Andersson I, Ikeda DM, Zackrisson S, et al. (2008) Tomosynthesis and digital mammography: a comparison of breast cancer visibility and BIRADS classification in a population of cancers with subtle mammographic findings. Eur Radiol 18: 2817–2825.
80. Wallis MG, Moa E, Zanca F, et al. (2012) Two-view and single-view tomosynthesis versus full-field digital mammography: high-resolution X-ray imaging observer study. Radiology 262: 788–796.
81. Gennaro G, Hendrick RE, Ruppel P, et al. (2013) Performance comparison of single-view digital breast tomosynthesis plus single-view digital mammography with two-view digital mammography. Eur Radiol 23: 664–672. doi:10.1007/s00330-012-2649-1.
82. Zuley ML, Guo B, Catullo VJ, et al. (2014) Comparison of Two-dimensional Synthesized Mammograms versus Original Digital Mammograms Alone and in Combination with Tomosynthesis Images. Radiology: published online ahead of print.
83. Skaane P, Gullien R, Eben EB, et al. (n.d.) Implementation of synthesized 2D Plus tomosynthesis images in breast cancer screening: comparison of performance levels with full field digital mammography plus tomosynthesis in a population-based screening program. Presented At: Radiological Society of North America 2013 Scientific Asembly and Annual Meeting, December 1-6, 2013, Chicago, IL.
84. Schie G Van, Mann R, Imhof-Tas M, et al. (2013) Generating synthetic mammograms from reconstructed tomosynthesis volumes. IEEE Trans Med Imag 32: 2322–2331.
85. Zuley ML, Bandos AI, Abrams GS, et al. (2010) Time to diagnosis and performance levels during repeat interpretations of digital breast tomosynthesis: preliminary observations. Acad Radiol 17: 450–455. doi:10.1016/j.acra.2009.11.011.
86. Dang PA, Freer PE, Humphrey KL, et al. (2014) Addition of Tomosynthesis to Conventional Digital Mammography: Effect on Image Interpretation Time of Screening Examinations. Radiology 270: 49–56.
87. Van Schie G, Wallis MG, Leifland K, et al. (2013) Mass detection in reconstructed digital breast tomosynthesis volumes with a computer-aided detection system trained on 2D mammograms. Med Phys 40: 041902. doi:10.1118/1.4791643.
88. Chan H-P, Wei J, Zhang Y, et al. (2008) Computer-aided detection of masses in digital tomosynthesis mammography: Comparison of three approaches. Med Phys 35: 4087–4095. doi:10.1118/1.2968098.
89. Chan H-P, Wu Y-T, Sahiner B, et al. (2010) Characterization of masses in digital breast tomosynthesis: Comparison of machine learning in projection views and reconstructed slices. Med Phys 37: 3576–3586. doi:10.1118/1.3432570.
90. Reiser I, Nishikawa RM, Giger ML, et al. (2006) Computerized mass detection for digital breast tomosynthesis directly from the projection images. Med Phys 33: 482–491. doi:10.1118/1.2163390.

Contacts of the corresponding author:

Author: Ingrid Reiser
Institute: The University of Chicago
Street: 5841 S. Maryland Ave
City: Chicago, IL 60637
Country: US
Email: ireiser@uchicago.edu